Structural characterization of a Mo/Si multilayer reflector by means of x-ray diffraction measurements

Dong-Eon Kim,[a] Dong-Ho Cha, and Sang-Won Lee
Physics Department, Pohang University of Science and Technology, San 31 Hyoja-Dong, Pohang, Kyungbuk 790-784, Korea

(Received 9 August 1996; accepted 10 January 1997)

The physical and optical characteristics of a multilayered synthetic microstructure (MLSM) have a significant structural dependence. Knowledge of the structure and its correlation to physical properties is needed in order to control the fabrication of MLSMs to obtain desired properties. Important parameters for the description of the structure are the thickness of a repeating unit, the thickness ratio of composite materials within the repeating unit and the degree of interdiffusion and roughness at interfaces. The effects of these various structural parameters on the small-angle x-ray diffraction (XRD) pattern are investigated for a molybdenum-silicon MLSM. The angular positions of the Bragg peaks are sensitive to the thickness of the repeating unit (Mo/Si bilayer in this study), and the pattern of the subsidiary peaks in the low-order Bragg region has a strong dependence on the thickness ratio. The major effect of interfacial diffusion is the overall reduction of the intensities of high-order Bragg peaks. However, the atomic concentration profile correlates with their relative intensities. The uncorrelated roughness is responsible for the increased linewidths of the Bragg peaks and the increase of the relative intensities of the subsidiary peaks to those of the Bragg peaks. Based on the above results, we present an analysis of the experimental XRD data in order to deduce the structural parameters of a molybdenum-silicon MLSM. © *1997 American Vacuum Society.* [S0734-2101(97)00204-2]

I. INTRODUCTION

During the past few decades vacuum thin-film fabrication technology has advanced to a degree that nanometer-scale thin-film structures are routinely produced in a controlled manner. The close proximity of different thin-film materials provides the opportunity to study novel physical characteristics that are much different from their bulk properties. Multilayered synthetic microstructures (MLSMs) have been investigated in various scientific fields such as opto-magnetism, x-ray optics, and giant magnetoresistance.[1]

To understand and control the optical and/or physical properties of a MLSM and to fabricate a better MLSM, one should be able to determine the structural parameters and correlate them with experimentally observed physical data. The structure has been investigated by using transmission electron microscopy (TEM), x-ray diffraction (XRD), large-angle XRD, Rutherford backscattering spectroscopy (RBS), and Auger depth profiling. TEM and XRD have most commonly been utilized to study the structure of MLSMs. The TEM gives us a direct image of the cross section at the cost of sample destruction. However, the image presents information only on a localized area, and due to the nonlinear scattering of electrons with high atomic-number elements, special care should be taken to interpret the TEM data to extract quantitative information of the structure.[2] XRD is a promising technique for characterizing structures. It is nondestructive so that it can be used for *in situ* measurements. The relatively small x-ray wavelength allows us to study spatial variations down to atomic dimensions. X rays have a penetrating ability, allowing analysis of sub-surface regions as well. However, interpretation of the XRD data and extraction of reliable quantitative information concerning the structural parameters have been limited due to the lack of a quantitative model which can incorporate the realistic interfaces into computation. Recently, much attention has been paid to x-ray scattering from the interfaces of nonideal multilayer structures and progress has been made on the interpretation of the XRD data and the acquisition of more reliable data on the structures.[3–6]

Figure 1 shows the experimental small-angle XRD pattern of a 30-bilayer Mo/Si MLSM obtained using Cu K_α (0.154 nm) radiation. The XRD pattern is dominated by the strong Bragg peaks (reflections) and subsidiary peaks between the consecutive Bragg peaks, and their variations in intensities and positions. The Bragg peaks result from the complete constructive interference between x rays reflected by each of the multilayer interfaces; on the other hand, the subsidiary peaks arise from the incomplete interference. Quantitative analysis of this data should be able to explain the following features:

(1) the positions of the Bragg peaks,
(2) the relative intensities of the Bragg peaks,
(3) the widths of the Bragg peaks,
(4) the shape and intensities of the subsidiary peaks.

In this article, we present the theoretical simulations of the effects of various structural parameters of a Mo/Si MLSM on the XRD pattern. The results are used to characterize the structure of a Mo/Si MLSM. In Sec. II, a theoretical model for computation is described. The effects of the

[a]Electronic mail: kimd@vision.postech.ac.kr

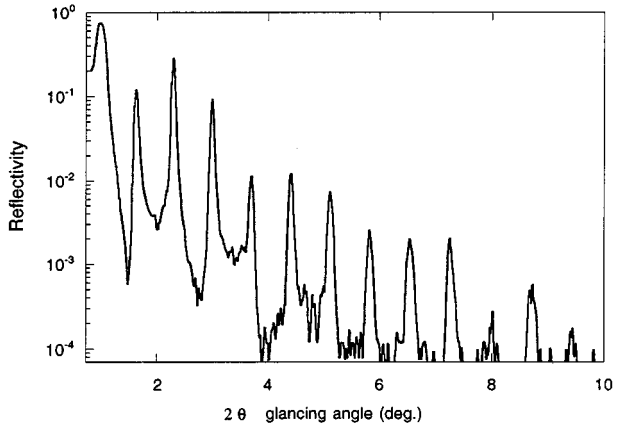

FIG. 1. Experimental XRD pattern of a Mo/Si MLSM using Cu K_α 0.154 nm.

structural parameters on the XRD data are discussed in Sec. III. Section IV deals with application to the structural characterization of a Mo/Si MLSM.

II. SIMULATION MODEL

An MLSM as a x-ray reflector consists of alternating layers of two different materials: Mo and Si for the present study. In MLSMs, there are always imperfections at interfaces. Roughness and interdiffusion co-exist at interfaces and are major defects that affect most of the physical properties. A Debye–Waller approach has been used to incorporate their effects on the XRD pattern.[4,7,8] The treatment implicitly assumes that the MLSM structure is perfectly coherent and the extent of interdiffusion of both materials is the same. Hence the approach cannot explain the experimental XRD data in detail since they contain contributions from the incoherence of the inner structure. One feature which the approach fails to describe is the decrease of the intensities of the subsidiary peaks relative to the Bragg peaks.[3] This approach also does not account for the broadening of the high-order Bragg peaks. Slaughter *et al.*[4] have studied different structural models such as the trilayer model and the graded-roughness bilayer model for fitting the Bragg peaks. Since a Debye–Waller approach was used for the interface profile, there was still a relatively large discrepancy in the simulation of the subsidiary peaks.

In our simulation, interdiffusion and roughness are separately treated and their respective effects on the XRD data are studied. The classical interdiffusion of two materials due to the interaction of surface species upon heating the film produces a variation in composition at interface. Such a profile is governed by Fick's second law of diffusion:

$$\frac{\partial n_i(z,t)}{\partial t} = D_i \frac{\partial^2 n_i(z,t)}{\partial z^2}, \tag{1}$$

where n_i is the atomic concentration of a particular element i, and D_i is its diffusion coefficient. This equation assumes that the diffusion takes place due to the random walk processes of individual atoms at interface. The solution of this equation is given by

$$n_i(z,t) = \frac{1}{\sqrt{2\pi}\sigma_i} \int_{-\infty}^{+\infty} n_i(\xi,0) \exp[-(z-\xi)^2/2\sigma_i^2] d\xi, \tag{2}$$

where $\sigma_i = \sqrt{2D_i t}$ is the rms value of diffusion length. Consider an interface between the film components A and B. Assume that the initial profile of the atomic concentration is a square well when there is no diffusion, i.e.,

$$n_A(z,0) = n_{A0}, \quad n_B(z,0) = 0 \quad (0 < z < d_A)$$
$$n_A(z,0) = 0, \quad n_B(z,0) = n_{B0} \quad (d_A < z < d),$$

where n_{A0} and n_{B0} are the pure atomic concentrations of A and B elements, respectively. d_A is the thickness of the A layer and d is the bilayer thickness. Then the diffusion changes the square well profile to the following profile:

$$n_A(z,\sigma_A) = n_{A0} \frac{1}{\sqrt{2\pi}\sigma_A} \int_0^{d_A} \exp[-(z-\xi)^2/2\sigma_A^2] d\xi$$

$$n_B(z,\sigma_B) = n_{B0} \frac{1}{\sqrt{2\pi}\sigma_B} \int_{d_A}^{d} \exp[-(z-\xi)^2/2\sigma_B^2] d\xi \tag{3}$$

for the diffusion lengths of σ_A and σ_B, respectively. Various interface profiles of the atomic concentration for the different values of σ_A and σ_B can be produced as shown in Fig. 2. In our calculation, the interface profile was divided into many slabs. The number of the slabs was large enough to properly represent the interface profile. The atomic concentration or the index of refraction of a slab was evaluated at its center. The x-ray scattering from interfaces between the slabs has been calculated using a recursive method, suggested by Parratt,[9] and further developed by Underwood and Barbee,[10] which includes multiple scattering between interfaces. For a given interface profile, the index of refraction can be found by the following equation:

$$\hat{n}(z) = 1 - \frac{r_0 \lambda^2}{2\pi} \{[(n_A(z) f_A + n_B(z) f_B] + i[n_A(z) f_A' + n_B(z) f_B']\}, \tag{4}$$

where $f_{A,B}$ and $f'_{A,B}$ are the real and imaginary parts of the atomic scattering factor of the elements A and B, respectively. r_0 is the classical electron radius.

The roughness at interface can be largely divided into two categories: correlated roughness and uncorrelated roughness. The correlated roughness propagates from interface to interface. This type of roughness results from digs or scratches on a substrate and produces an averaged effect by interdiffusion. On the other hand, the variation in the thickness of each layer, the local interdiffusion at the interface during the deposition, and roughness due to island growth during the deposition are mainly responsible for the uncorrelated roughness. The lateral domain sizes of these variations are usually large compared to the wavelength of the diffracting radiation (in this case, 0.154 nm). An XRD diffraction pattern can then

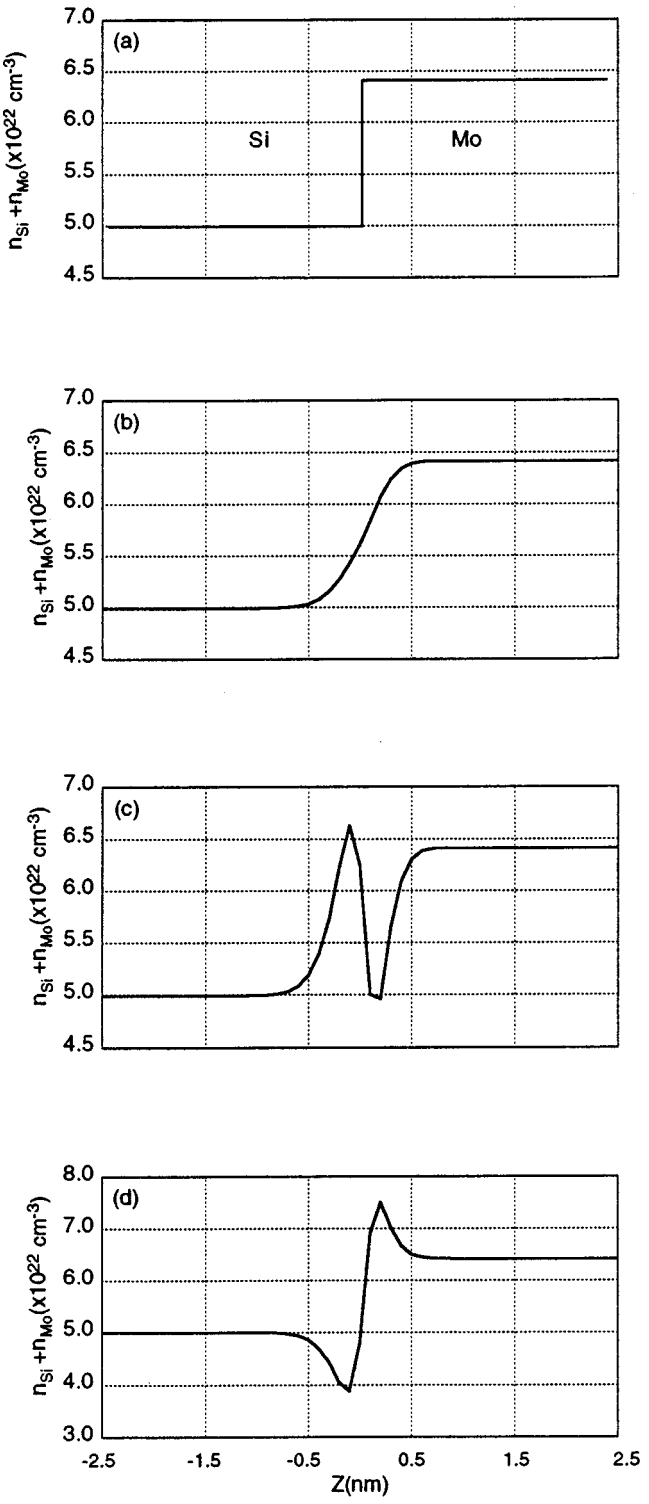

FIG. 2. Atom concentration profiles for various diffusion parameters. σ_{Si} (nm), σ_{Mo} (nm): (a) 0.0, 0.0; (b) 0.3, 0.3; (c) 0.1, 0.3; and (d) 0.3, 0.1.

be approximated by the average pattern for a group of MLSMs in which bilayer thicknesses vary randomly within a given error range. The XRD patterns are calculated as a function of angle for such a group of MLSMs and then added together and divided by the number of the group members to obtain an average XRD pattern:

$$I=\frac{1}{k}\sum_{i=1}^{k} I_i(d_0\pm\delta_j),\quad j=1,2,\ldots,N, \tag{5}$$

where k is the number of the members of the group of MLSMs, d_0 the average bilayer thickness, δ_j the random thickness error in the jth layer, and N the total number of bilayers.

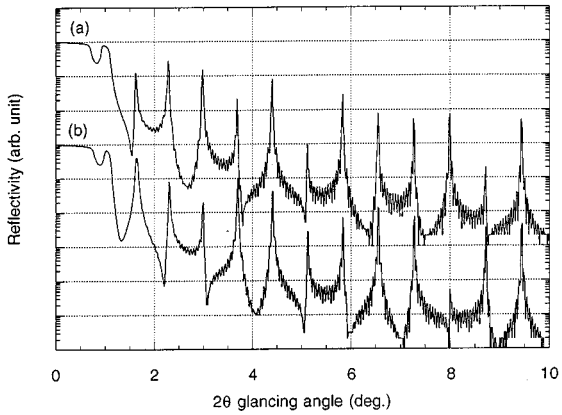

FIG. 3. The change of XRD pattern with respect to the thickness ratio, γ: (a) $\gamma=0.58$, (b) $\gamma=0.73$. $d=12.202$ nm and $N=30$.

III. STRUCTURAL EFFECTS ON XRD PATTERN

The small-angle XRD pattern is very sensitive to structural parameters. In the case of a Mo/Si MLSM, for example, the bilayer thickness $d(=d_{Mo}+d_{Si})$, the thickness ratio of the Mo layer to the bilayer thickness $\gamma(=d_{Mo}/d)$, the interdiffusion lengths σ's, and the roughness δ at interfaces are the parameters that most affect the XRD pattern. In general, the combined effect of the above structural parameters is very complicated. If we know the features of the effect that each structural parameter makes on an XRD pattern, we are able to devise a method or procedure to extract the structural information from given experimental XRD data. It is therefore necessary to find out the effect of each structural parameter on the XRD pattern.

The bilayer thickness and the thickness ratio are the most important parameters to be determined first. Using the refraction-corrected equation for the Bragg condition, both the average bilayer thickness and the thickness ratio can be estimated from the angular positions of the Bragg peaks, assuming that the interface is abrupt.[11] These values are used as input values for the calculation of the XRD pattern for comparison with an experimental XRD pattern.

Figure 3 shows the change of the XRD pattern of an ideal MLSM with respect to the variation of γ and illustrates the effect of different γ's. In Figs. 3(a) and 3(b) the dramatic difference between the Bragg peaks can be noticed especially in the small-angle region. The reason for this is due to the change of the relative phases between the electromagnetic fields reflected at consecutive sublayers owing to the varia-

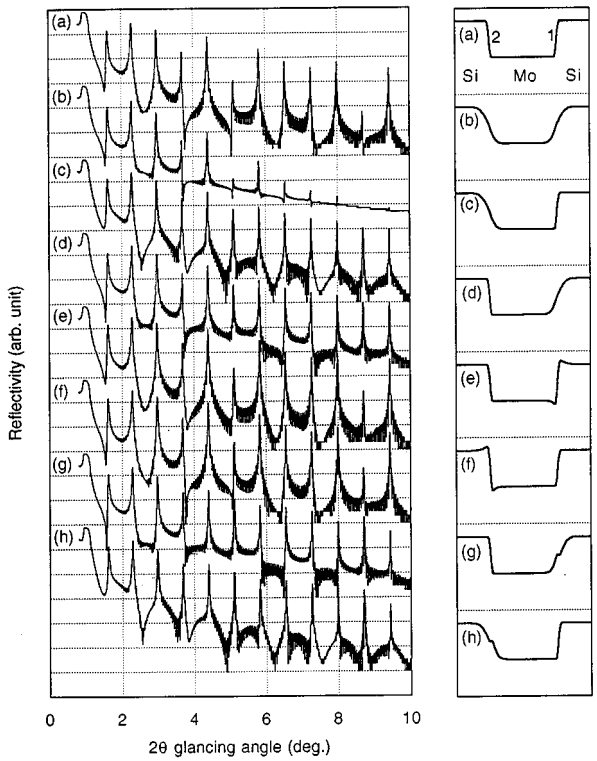

FIG. 4. Variation of the XRD pattern as a function of diffusion lengths for a given set of $d=12.202$ nm, $N=30$, and $\gamma=0.58$. The corresponding atomic concentration profiles of Mo and Si are also shown. The scale of the concentration profiles is the same as shown in Fig. 2. $\sigma_{Si,1}$ (nm), $\sigma_{Mo,1}$ (nm), $\sigma_{Si,2}$ (nm), $\sigma_{Mo,2}$ (nm): (a) 0.1, 0.1, 0.1, 0.1; (b) 0.5, 0.5, 0.5, 0.5; (c) 0.1, 0.1, 0.5, 0.5; (d) 0.5, 0.5, 0.1, 0.1; (e) 0.5, 0.1, 0.1, 0.1; (f) 0.1, 0.1, 0.5, 0.1; (g) 0.1, 0.5, 0.1, 0.1; and (h) 0.1, 0.1, 0.1, 0.5.

tion of γ. Both the relative intensities of the Bragg peaks and the shape of the subsidiary peak change; however, the positions of the Bragg peaks do not change. This fact can be utilized to refine the value of γ.

The effect of diffusion at interfaces on an XRD pattern is shown in Fig. 4. Figure 4 shows XRD patterns of a MLSM for various atomic concentration profiles at the interface. At an interface the diffusion rate of silicon into molybdenum is not necessarily the same as that of molybdenum into silicon. Hence the atomic concentration profile at an interface is controlled by two parameters (σ_{Mo} and σ_{Si}). In the repeating unit of a Mo/Si MLSM, there are two interfaces: Si-on-Mo (called interface 1) and Mo-on-Si (called interface 2) interfaces. Since they are formed at different times and under different conditions, the diffusion lengths at interface 1 do not need to be the same as those at interface 2. The interface profiles of the repeating unit of a Mo/Si MLSM are, therefore, governed by four parameters: $\sigma_{Si,1}$, $\sigma_{Si,2}$, $\sigma_{Mo,1}$, and $\sigma_{Mo,2}$, where $\sigma_{Si,1}$, for example, represents the diffusion length of silicon into molybdenum at interface 1. The interface profiles calculated by using Eq. (3) for different values of diffusion lengths are also shown in Fig. 4.

Figures 4(a) and 4(b) show XRD data from interface profiles for the case that the diffusion lengths of silicon into molybdenum and molybdenum into silicon are the same at the interface. This is the same profile as given by an error function which has been commonly used. Using the Debye–Waller approach which was shown to be valid for this kind of profile,[5] the calculation of XRD patterns can be quite easily done. As the diffusion length is increased, the intensities of the Bragg peaks decrease. The larger the angle is, the severer the reduction of the intensities is for a given diffusion length.

The interface profile of the Mo-on-Si has been known to be different from that of Si-on-Mo. In general, the diffusion lengths between the Mo-on-Si interface and the Si-on-Mo interface may be different. The simulated results for the different diffusion lengths are shown in Figs. 4(c) and 4(d). Comparing these with those from centrosymmetric profiles [Figs. 4(a) and 4(b)], it is noticed that the general shapes of the subsidiary peaks show little change; however, the intensities of the high-order Bragg peaks increase dramatically. Interestingly, the 7th and 12th Bragg peaks show the most significant change between the centrosymmetric and the noncentrosymmetric profiles.

Figures 4(e)–4(h) show the effect on the XRD pattern due to the change of the individual diffusion lengths at both interfaces ($\sigma_{Si,1}$, $\sigma_{Si,2}$, $\sigma_{Mo,1}$ and $\sigma_{Mo,2}$). Figure 4(e) is the case where only $\sigma_{Si,1}$ is different from others. The change of $\sigma_{Si,1}$ gives rise to the slight increase of the intensities of the Bragg peaks, compared to Fig. 4(a). The increase is larger for the high-order peaks than for the low-order peaks. The effect due to a change of $\sigma_{Si,2}$ is shown in Fig. 4(f). The interface profile looks the same as that in Fig. 4(e) except that the interfaces are exchanged. The XRD pattern is also almost similar to that in Fig. 4(e) except for the slightly different shape of the subsidiary peaks in several regions due to the phase difference. As can be noticed in Figs. 4(e) and 4(g), the change of the diffusion lengths of molybdenum brings about bigger effects on the XRD patterns, especially, in the relative intensities of the Bragg peaks. These observations, therefore, suggest that the relative intensities of the Bragg peaks are sensitive to the atomic concentration profile at the interfaces.

The effects of uncorrelated roughness on the XRD data are presented in Fig. 5. The existence of the roughness keeps the phase differences between the consecutive layers from being maintained but forces them to randomly vary, leading to irregular maxima peaks. Hence when many of such patterns are averaged, the subsidiary peaks smear out and their oscillatory behavior disappears. The intensities of the Bragg peaks reduce but their widths increase. The roughness also increases the intensities of the subsidiary peaks so that in the large-angle region, the ratio of the intensities of the subsidiary peaks to those of the Bragg peaks gets larger. For a mixed coherence case where the thickness ratio of Mo and Si within a repeating unit is kept unchanged but thickness of the repeating unit changes randomly, similar results are expected, but with less effects.

In summary, the thickness ratio predominantly affects the shape of XRD features principally in the small-angle region. Hence the thickness ratio can be estimated by fitting the

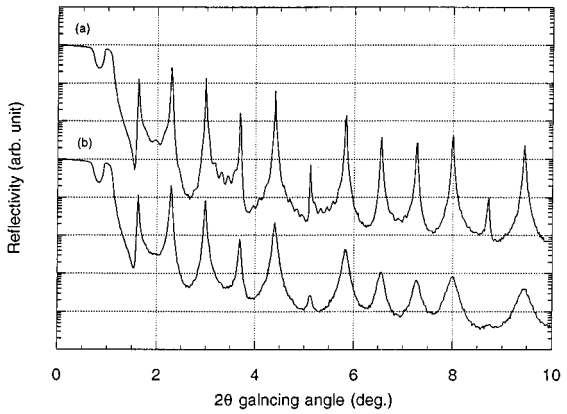

FIG. 5. The change of XRD pattern with respect to the change of uncorrelated roughness: (a) δ=0.1 nm, (b) δ=0.3 nm. d=12.202 nm, N=30, and γ=0.58.

computer-generated XRD pattern to the experimentally determined pattern in the small-angle region. Both the interdiffusion and the roughness decrease the intensities of the Bragg peaks. However, the broadening of the widths of the Bragg peaks is mainly due to the uncorrelated roughness. This fact can be utilized for the estimation of the roughness. The degree of the interdiffusion can then be found by comparing the intensities of the Bragg peaks between the computer-generated and the experimental data and by taking into account the reduction of the intensities due to the roughness.

IV. APPLICATION TO EXPERIMENTAL XRD DATA

A Mo/Si MLSM used in this study was fabricated using a rf magnetron sputtering system with argon gas.[11] 30 Mo/Si layers were deposited on Si wafers. The XRD data obtained with Cu K_α (λ=0.154 nm) can be seen in Fig. 1. With the help of the refraction-corrected Bragg condition, the angular positions of the Bragg peaks can provide us with the average bilayer thickness, and the thickness ratio of a Mo sublayer to the bilayer.[4,11] These values are only approximate. Using these values as initial input values to the computer program for simulating XRD patterns, the fitting of the angular positions of the Bragg peaks and the shapes in the small-angle region to the experimental XRD data yields more accurate average bilayer thickness as well as the thickness ratio. Since the angular positions of the Bragg peaks and the shape of the subsidiary peaks depends on the bilayer thickness and the thickness ratio for a fixed average bilayer thickness, only proper values for both the thickness ratio and the average bilayer thickness result in a good fit of the calculated XRD pattern to the experimental pattern. The best fit was made for d=12.202 nm and γ=0.58. This bilayer thickness agrees with the values (12.0–12.5 nm) measured by TEM within experimental error.

As noticed in Sec. III, the effects due to uncorrelated roughness are different from those due to interdiffusion. The most important difference is that the broadening of the Bragg

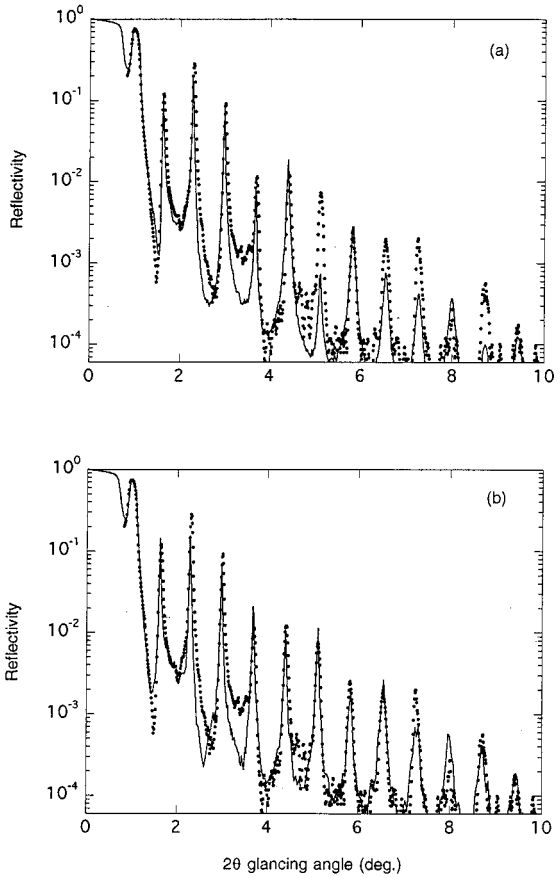

FIG. 6. Comparison of the best-fit calculated XRD pattern with an experimental XRD pattern (dots): (a) a calculated XRD pattern for d=12.202 nm, N=30, γ=0.58, $\sigma_{Si,1}=\sigma_{Mo,1}$=0.1 nm, $\sigma_{Si,2}=\sigma_{Mo,2}$=0.3 nm, and δ=0.25 nm. (b) A calculated XRD pattern for d=12.202 nm, N=30, γ=0.58, $\sigma_{Si,1}$=0.5 nm, $\sigma_{Mo,1}$=0.1 nm, $\sigma_{Si,2}$=0.1 nm, $\sigma_{Mo,2}$=0.6 nm, and δ=0.25 nm.

peaks is mainly due to the uncorrelated roughness. This unique characteristic can be used to estimate the degree of roughness by fitting the widths of the Bragg peaks and the intensities of the subsidiary peaks. The best fitted parameter for roughness was found to be δ=0.25 nm. However, with the use of only the uncorrelated roughness there are still differences especially between the intensities of the Bragg peaks. Since the main effect due to interdiffusion is the decrease of intensities of the Bragg and subsidiary peaks, the interdiffusion length can be further used to achieve a better fit.

Figure 6 shows the experimental XRD pattern and the best-fit calculated XRD patterns for the two cases. Figure 6(a) was obtained with $\sigma_{Si,1}=\sigma_{Mo,1}=\sigma_{Si/Mo}$=0.1 nm and $\sigma_{Si,2}=\sigma_{Mo,2}=\sigma_{Mo/Si}$=0.3 nm. This case assumes that the diffusion lengths of molybdenum into silicon and silicon into molybdenum at each interface within a repeating unit are the same. The different values of $\sigma_{Si/Mo}$ and $\sigma_{Mo/Si}$ indicate that the diffusion rate of a Si layer into a Mo layer during the deposition is different from that of a Mo layer into a Si layer. The above results show that there is a deeper diffusion at the interface of Mo-on-Si than at the Si-on-Mo interface, which

agrees with previous observations.[12,13] The agreement with the experimental data in the small-angle region is fair; however, there are still discrepancies in the large-angle region; especially, in the intensities of the 7th, 9th, 10th, 11th, and 12th Bragg peaks. This is due to the fact that the profile was limited because of the assumption that the diffusion rates of Si-into-Mo and Mo-into-Si at the interface are the same. In reality, the two diffusion rates can be different from each other. In this case, the interface profile is characterized by two parameters and can be much different from that given by the error function, as discussed previously. The best-fit calculated XRD pattern in the case of four independent parameters for diffusion lengths is shown in Fig. 6(b). Note that the intensities of the 7th, 9th, 10th, 11th, and 12th Bragg peaks now become closer to the experimental pattern than in the case of the conventional interface profile using a single diffusion parameter.

V. CONCLUSION

Through the simulation of the XRD pattern associated with a MLSM, the effects by various structural parameters such as bilayer thickness, the thickness ratio of constituent materials, interdiffusion and uncorrelated roughness have been investigated. The angular positions of the Bragg peaks yield the average bilayer thickness. The XRD pattern in the small-angle region is sensitive to the thickness ratio of constituent layers. Interdiffusion decreases the intensities of both the Bragg and subsidiary peaks but has no relevance to the widths of the Bragg peaks. The broadening of the Bragg peaks is mainly due to uncorrelated roughness. These characteristics of each structural parameter have been applied to analyze the structure of a Mo/Si MLSM fabricated by a magnetron sputtering system. Separate controls over diffusion lengths at each interface can provide better agreement between the experimental data and the simulation, thereby yielding more accurate structural parameters.

ACKNOWLEDGMENTS

This work has been supported by a grant from POSCON Co., the basic research program, POSTECH, Pohang, Korea, 1995, and in part under contract from Electronics and Telecommunications Research Institute.

[1]*Proceedings of the SPIE*, edited by Richard B. Hoover and Arthur N. C. Walker, Jr. (SPIE, Bellingham, WA, 1995); Gary A. Prinz, Physics Today **48**, 58 (1995).
[2]Y. Cheng, D. J. Smith, M. B. Stearns, and D. G. Stearns, J. Appl. Phys. **72**, 5165 (1992).
[3]Z. Xu, Z. Tang, and S. Kevan, J. Appl. Phys. **74**, 905 (1993).
[4]J. M. Slaughter, D. Schulze, C. R. Hills, A. Mirone, R. Stalio, R. N. Watts, C. Tario, T. B. Lucatorto, M. Krumrey, P. Mueller, and C. Falco, J. Appl. Phys. **76**, 2144 (1994).
[5]D. G. Stearns, J. Appl. Phys. **65**, 491 (1989).
[6]D. G. Stearns, J. Appl. Phys. **71**, 4286 (1992).
[7]L. Névot, B. Pardo, and J. Corno, Rev. Phys. Appl. **23**, 1675 (1988).
[8]E. Spiller and A. E. Rosenbluth, Proc. SPIE **563**, 221 (1985).
[9]L. G. Parratt, Phys. Rev. **95**, 359 (1954).
[10]J. H. Underwood and T. W. Barbee, Appl. Optics **20**, 3027 (1981).
[11]D. Kim, H. W. Lee, J. J. Lee, J. H. Lee, M. Sakurai, and M. Watanabe, J. Vac. Sci. Technol. A **21**, 148 (1994).
[12]D. G. Stearns, M. B. Sterns, Y. Cheng, J. H. Stith, and N. M. Ceglio, J. Appl. Phys. **67**, 2415 (1990).
[13]U. Kleineberg, H.-J. Stock, A. Kloidt, B. Schmiedeskamp, U. Heinzmann, S. Hopfe, and R. Scholz, Physica Status Solidi A **145**, 539 (1994).